![NIST logo] National Institute of Standards and Technology • U.S. Department of Commerce

Report of Test

Absolute Spectral Radiance Responsivity

of the

GLAMR exIGA Radiometer
Model L-1 8350, S/N 002

Request Submitted by:

Joel McCorkle
NASA Goddard Space Flight Center
Greenbelt, MD

1. Description of Calibration Items

The device under test (DUT) is an extended-indium gallium arsenide (ex-IGA) radiance meter manufactured by L-1 Standards and Technology, Inc. (L-1), model 8350, S/N 002 and referred to as GLAMR exIGA in this report. The device is housed in a 2-inch diameter tube with fore-optics consisting of two apertures to form a Gershun-tube radiometer. The detector is temperature controlled (L-1 model 3100-1L, S/N 12132) and the rear of the device has inputs for the L-1 temperature controller and a BNC output for the detector signal. The temperature controller was operated with the setpoint at -20.0 ℃ and maintained the temperature at -20.0 ℃. The detector came with a transimpedance amplifier (L-1 model 3300v2, S/N 008) which was used for the calibration. Figure 1.1 shows the detector and accessory equipment as received.

Figure 1.1 Photographs of the GLAMR ex-IGA detector as received. The temperature controller (left) and transimpedance amplifier (middle) were received with the same devices associated with the silicon and IGA radiometers. The GLAMR ex-IGA radiance meter was received packaged in a pelican case (right).

1.1 Calibration Request

The request was to calibrate the DUT for absolute radiance responsivity from 1600 nm to 2500 nm with a standard uncertainty of 1.0 % (k=1) or better from 1600 nm to 2300 nm and 10 % or better from 2300 nm to 2500 nm.

2. Description of Test

The detector was characterized for absolute spectral radiance responsivity on the NIST facility for Spectral Irradiance and Radiance responsivity Calibrations using Uniform Sources (SIRCUS).[1,2] The calibration took place in various stages from April 19, 2021 to May 03, 2021. During each calibration test, the detector was temperature controlled with setpoint at -20.0 °C by the L-1 controller. The calibration was completed using reference detector "SIRCUS Pyro #1 5mm." Use of this pyroelectric detector allows traceability to the NIST Primary Optical Watt Radiometer[3] (POWR) via the calibration of the pyroelectric detector against a silicon trap detector (T-06 calibration from POWR in 2016[4]) from 600 nm to 900 nm and a calibration of its reflectance[5,6] completed in autumn 2020.[7]

Description of laser systems used: Several laser systems were used to cover the specified ranges for the various parts of the calibration.

1. A picosecond mode-locked LBO-OPO laser was used from 1588 nm to 1670 nm using the idler output from the main cavity.
2. Argos SF-15 Module B (CW) from 1633 nm to 1880 nm using the signal output.
3. IPG Cr^{2+}:ZnS/Se laser (CW) from 1880 nm to 2512 nm.

Each laser was coupled to an optical fiber connected to the side port of the integrating sphere, where the coupled laser illuminates an area toward the front of the sphere. Other optical laser components generally include a speckle-reduction device, a laser power controller, and a wavemeter.

For the LBO-OPO, the optical fiber was Low-OH silica fiber, but no speckle reduction device was employed because the laser bandwidth is broad enough to inherently reduce speckle. A Bristol 621 wavemeter (S/N: 6208) was used to directly measure the wavelength of the signal beam oscillated by the main cavity. The signal beam wavelength measured by the wavemeter was converted to the idler wavelength, λ_{idler}, using the relation given by equation 2.1,

$$\lambda_{idler} = \frac{1}{\left(\frac{1}{\lambda_{pump}} - \frac{1}{\lambda_{signal}}\right)} \qquad (2.1)$$

where λ_{pump} is 532.2 nm and λ_{signal} is the vacuum wavelength measured by the Bristol wavemeter. The vacuum wavelengths were converted to the air value for data analysis by dividing by a factor of 1.00027.

For the Argos and IPG lasers, the optical fiber was 200 μm core diameter ZrF_4 fiber. No speckle reduction device was used in conjunction with these lasers because no such device was available that operates in the associated wavelength range. A Burleigh wavemeter (S/N: 0024213) measured the air wavelength for these lasers.

A laser power controller was not used for several reasons. One, the device performed poorly with

chopped signals generated by our setup where the time constant required for the signal to stabilize was too long. The pyroelectric detector is optimally chopped at ~ 10 Hz and it takes a considerable amount of the 100 ms chopped pulse duration for the beam to stabilize. Two, the laser power controller considerably attenuates the available laser power and reduces the signal available with the pyroelectric detector. The lower signal leads to higher measurement standard deviation due to the low signal-to-noise associated with the pyroelectric detector.

Integrating Sphere: The integrating sphere used for radiance responsivity was a Labsphere 30.48 cm (12") diameter Spectralon-coated sphere equipped with a 5.08 cm (2") diameter exit aperture fabricated by Labsphere (non-point source geometry).

Data Acquisition and Control Program: Use of the pyroelectric reference detector requires alternating current (AC) signal acquisition using an optical chopper. The chopper (Oriel Instruments Optical Chopper, M/N: 3502, S/N: 2095) operated at 10.7 Hz using a 50:50 wheel with 2 apertures and was placed in the laser beam path between the fiber coupler and laser power controller. The data was acquired using the LabVIEW program "SIRCUS chopping_V6.vi" which allows demodulation of the desired detector response signal from the chopped AC quasi-square waveform signal. Background signals are subtracted from the AC square waveform analysis when the chopper is in the "OFF" position. Chopped waveform signals were sequentially collected for each detector (DUT and reference standard) along with simultaneously recorded monitor signals into separate analog input channels (differential mode) of a National Instruments data acquisition (DAQ) module (M/N: NI USB-6211, S/N: 1A98ECC). The acquisitions are triggered using the reference chopper signal to the digital I/O input of the data acquisition module.

Each acquisition comprised of 10 second waveforms at 10 kHz sample collection rates for the detector and monitor yielding ~ 100 independent measurements of the source signal per waveform acquisition. Each cycle in the waveform is averaged and subtracted (ON-OFF) after removing 15 ms of data around the rising and falling edges of the waveform cycles. The ON-OFF signals are then divided by the similarly analyzed monitor waveform to determine the ratio (DUT/Mon) signals. The individual ratio signals within the single waveform acquisition are then averaged. The 10-second waveform acquisitions are also repeated multiple times to determine the final average and standard deviation of the mean.

Description of calibration detectors: The working standard reference detector, SIRCUS Pyro #1 (Gentec, M/N: SDX-1237, S/N: 507568 with power supply model: STEP, S/N: 507569), was used to measure the radiance and irradiance emitted from the source sphere from 900 nm to 1730 nm. It is a pyroelectric detector equipped with an aperture having a nominal diameter of 3.5 mm and has an internal amplifier with fixed gain. SIRCUS Pyro #1 was previously calibrated for irradiance responsivity from 500 nm to 3400 nm using two steps: In step one, a SIRCUS irradiance responsivity calibration was completed on SIRCUS Pyro #1 using a silicon trap detector, T-06, at tie points between 600 nm and 900 nm to set the irradiance scale. In step two, the directional hemispherical reflectance of a two witness detector samples for SIRCUS Pyro #1were measured in two ranges, 500 nm to 2500 nm and 830 nm to 3300 nm, to determine the spectral relative absorptance, which is proportional to the pyroelectric detector spectral responsivity.[7]

The monitor detector was a Mercury Cadmium Telluride (MCT) detector mounted directly to the source sphere. It was connected to a Stanford Research Systems current preamplifier (Model SR570, S/N: 57687).

3-axis stage: The integrating sphere is mounted on an XYZ translation stage, with the Z-position (along the optical axis) measured with a linear encoder. The X- and Y-axes enable the source to be properly positioned in front of an instrument before it measures the sphere radiance. The Z-position is used to accurately determine the separation between relevant apertures.

Measurement Setup: Detectors used in these experiments were mounted on tip-tilt stages and aligned to the optical axis of the integrating sphere source using a double-headed laser. To align the detectors to the sphere, the double-headed laser was first mounted in-front of the sphere where one end of the laser was previously aligned to the center of the sphere aperture. The other end of the laser was retroreflected from a glass microscope slide on each detector to align to the optical axis. Lastly, the laser was centered on each detector using the 3-axis stage to determine the X,Y position.

See Figure 2.1 for photographs of the measurement setup in the SIRCUS enclosure showing the detector bench setup in relation to the integrating sphere. Figure 2.2 shows the setup of the control boxes and Figure 2.3 shows the setup of the DAQ module. As shown in Figure 2.3, SIRCUS Pyro #1 was connected to analog input (ai) channel 2, while the monitor detector was connected to ai channel 0 and GLAMR exIGA was connected to ai channel 3. The chopper reference signal is connected to digital I/O input channel PFI0 and grounded to digital ground (DGND). Also of note, the pyroelectric detector was grounded from its BNC connector to a screw on an instrument rack using an alligator clip wire (black).
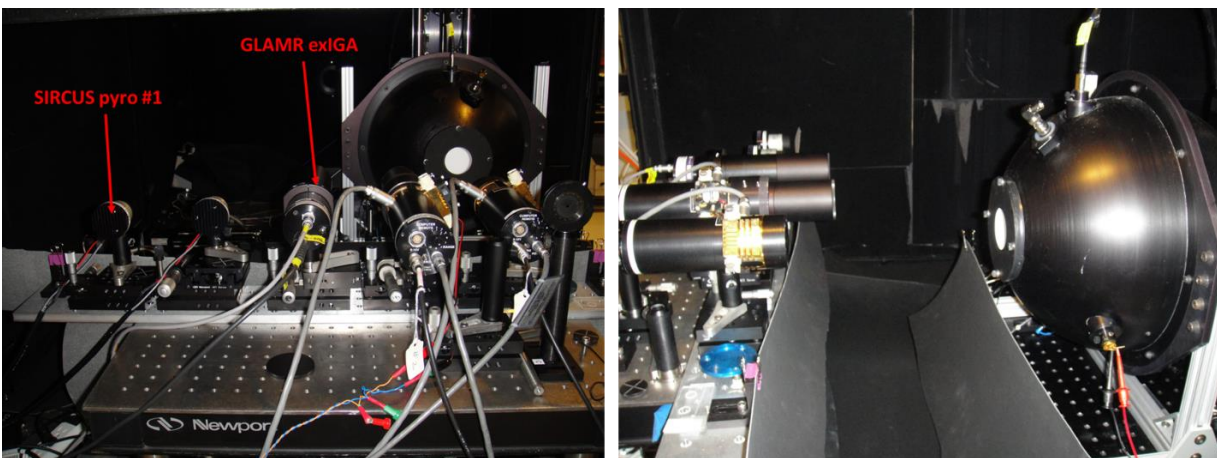

Figure 2.1 Photographs of the detector setup inside the SIRCUS enclosure: detector bench back-view (left), side-view (right). The detector bench also included a second pyroelectric detector (NASA Pyro #2) and NIST transfer detectors NS0103 and NS0104.

Figure 2.2 Photographs showing the control box setup for GLAMR including the transimpedance amplifiers and temperature controllers and the step controller for SIRCUS Pyro #1
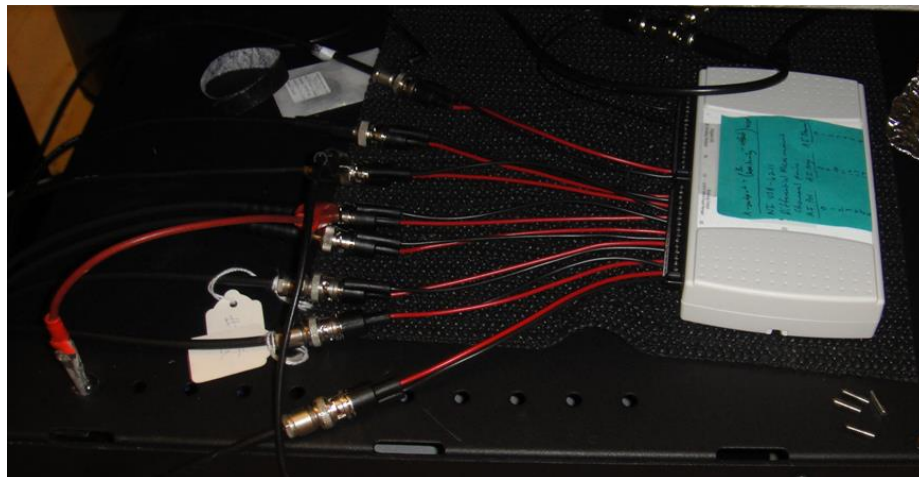

Figure 2.3 Photograph showing the setup of the National Instruments NI USB-6211 DAQ module including connection to the analog input channels and grounding wires

2.1 Radiance Responsivity Calibration of GLAMR exIGA from SIRCUS Pyro #1

Absolute radiance responsivity measurements of GLAMR exIGA (with associated transimpedance amplifier) versus SIRCUS Pyro #1, were completed at discrete wavelengths between 1588 nm to 2512 nm using the SIRCUS facility. The integrating sphere source (ISS) was the 30.5 cm (12")

diameter sphere described above with a 5.08 cm (2") aperture. The sphere was placed at a Z-position of -504.38 mm. This Z-position was approximately 20 cm away from the front aperture of the DUT, which placed the field of view completely within the sphere output aperture. An X-Y response map for the DUT was also measured, verifying the central position and underfilled configuration of the DUT relative to the sphere aperture. The sphere was placed at the same Z-position for measurements of the sphere radiance with SIRCUS Pyro #1. This placed the sphere aperture well within the acceptance angle of SIRCUS Pyro #1 for power measurement as suggested in Section 3.1, below. The working distance for SIRCUS Pyro #1 was determined from the sphere Z-position and the radiometrically determined detector position, as described in Section 3.2 below.

The pre-amplifier gain was 1 x 10^5 V/A for the GLAMR exIGA with multiplier set to 10 for all measurements. SIRCUS Pyro #1 has an internal amplifier with fixed gain.

3. Results of Test

For this test, a radiance calibration was performed. Here, the reference detector SIRCUS Pyro #1 establishes the radiance emitted from the source sphere. Even though SIRCUS Pyro #1 is an irradiance meter, it was used to determine the source radiance, requiring knowledge of the solid angle of the source. To determine the solid angle, the distance between the reference detector aperture and the integrating sphere source aperture was measured, along with the integrating sphere and trap detector aperture areas: See Section 3.1. The position of the reference detector was determined radiometrically, as described in Section 3.2, and therefore, the distance of the reference detector to the sphere source was determined by measuring the Z-position of the sphere with the linear encoder on the Z-axis stage.

3.1 Determination of the sphere source radiance

The radiance of the sphere source was determined with the flux transfer method. The reference detector SIRCUS Pyro #1 measured the radiant power from the sphere source passing through two precision apertures, one on the source side, another on the detector side.

The radiance L [W m^{-2} sr^{-1}] of the sphere was determined from radiant power P [W] and the geometric extent G by:

$$L = \frac{P}{G} \tag{3.1}$$

The geometric extent G [m^2 sr] is given by

$$G = \frac{\pi^2}{2}\left[(d^2 + r_s^2 + r_D^2) - \{(d^2 + r_s^2 + r_D^2)^2 - 4r_s^2 r_D^2\}^{1/2}\right] \tag{3.2}$$

where r_s is the radius of the aperture in front of the source, r_D is the radius of the aperture in front of the detector, and d is the distance between the two apertures. The diameter of the sphere aperture was large enough (50.8 mm) to overfill the radiance measurement angle of the DUT radiometer by the sphere output radiation. The distance, d, was chosen large enough (300.69 mm) so that the sphere aperture was well within the acceptance angle of the working reference detector (SIRCUS Pyro #1) for power measurement but also close enough to allow reasonable signal magnitude on the pyroelectric reference detector.

3.2 Detector offset and offset uncertainty determination for irradiance meters

When the working reference detector is an irradiance meter, both radiance and irradiance measurements of the sphere source require knowledge of a distance between the source and a detector aperture. For the radiance measurements performed in this calibration, the distance of the working reference detector, SIRCUS Pyro #1, was determined.

All distances were determined radiometrically. In general, at several different Z positions, the detector and monitor voltages were recorded to yield a relative irradiance. This was done using the optically chopped data acquisition method described in Section 2, above. Using the $1/Z^2$ law for on-axis irradiance (inverse square law) the resultant data can be fit by a point-source geometry (Equation 3.3) and a non-point-source geometry (the experimental configuration, Equation 3.4) to yield the Z-position of the detector aperture plane. From the Z-position encoder reading used in the radiance or irradiance measurements and the detector Z-position from the radiometric $1/Z^2$ law fit, the actual detector aperture to sphere aperture distance in millimeters (working distance) was determined. Figure 3.1 is a schematic of the configuration.

The inverse square law fitting equation for a point-source geometry is:

$$y = \frac{m_1}{\left(M_0 - m_2\right)^2} \qquad (3.3)$$

Where y is the relative irradiance, m_1 is a fitting constant, M_0 is Z-position of the integrating sphere that is read by the Z-encoder, and m_2 is the Z-position of zero offset between the two apertures. The fitting uncertainty in m_2, for the sphere position during calibration, gives the uncertainty in the distance s between the two apertures.
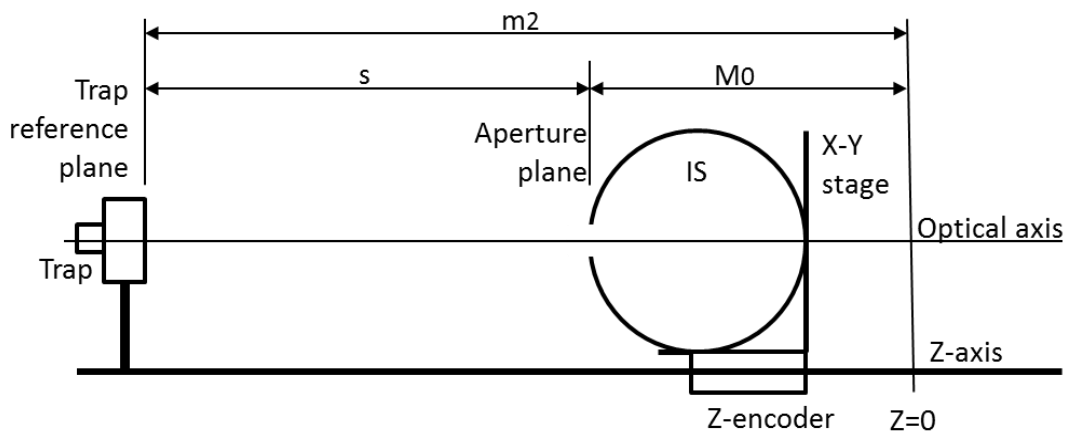

Figure 3.1. Schematic of the configuration for determining trap-sphere distance radiometrically.

If the source aperture is large, the non-point source geometry expression is fit to the data:

$$y = \frac{m_1}{((M_0 - m_2)^2 + m_3^2 + m_4^2)} \qquad (3.4)$$

where y, m_1, M_0, and m_2 are the same as in Eq. 3. $m_3 = r_d$, the radius of the detector aperture, and $m_4 = r_s$, the radius of the integrating sphere aperture. Equation 3.4 is valid in the limit where

$$(r_s^2 + r_d^2 + s^2) \gg 2r_s r_d \qquad (3.5)$$

and s is the distance between the source and detector apertures. The inverse square law measurements along with the fit of equation 3.4 to the data for each detector are shown in Figs. 3.2 and 3.3, below. At a separation, s, equal to the working distance, the ratio given by equation 3.5 was determined for each detector. This result is summarized in Table 3.1 and shows the condition of equation 3.5 holds and that equation 3.4 is valid in each case. The residuals are approximately 3 orders of magnitude smaller than the base measurement and show there is no obvious bias or offset. The fitting results are also summarized in Table 3.2.

Table 3.1 Results of Eq. 3.5 at minimum separation distances.

Detector	r_s (cm)	r_d (cm)	s (cm)	Ratio (Eq 3.5)
SIRCUS Pyro #1	2.54	0.175	30.069	1024

Table 3.2 Results of the inverse square law fits of equation 3.4 to the data.

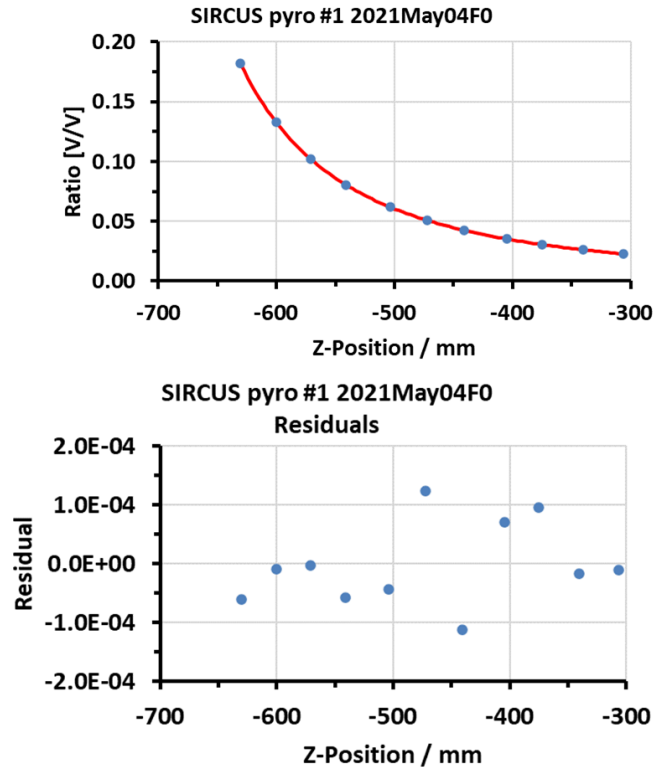| Detector	m_2 (mm)	Fitting Uncertainty (mm) (k=1)	R, fit
SIRCUS Pyro #1	-805.08	0.13667	1

Figure 3.2 Offset and uncertainty fit of the non-point source geometry equation 3.4 to the irradiance response data (upper) and residuals from the fit (lower) for SIRCUS Pyro #1 to determine distance for the radiance responsivity measurements.

3.3 Radiance responsivity of GLAMR exIGA from SIRCUS Pyro #1

Absolute spectral radiance responsivity of GLAMR exIGA was measured from 1588 nm to 2512 nm versus SIRCUS Pyro #1. This result is shown in Figure 3.4 and the tabulated data along with combined total uncertainty (k=1) is provided in Table 3.3.
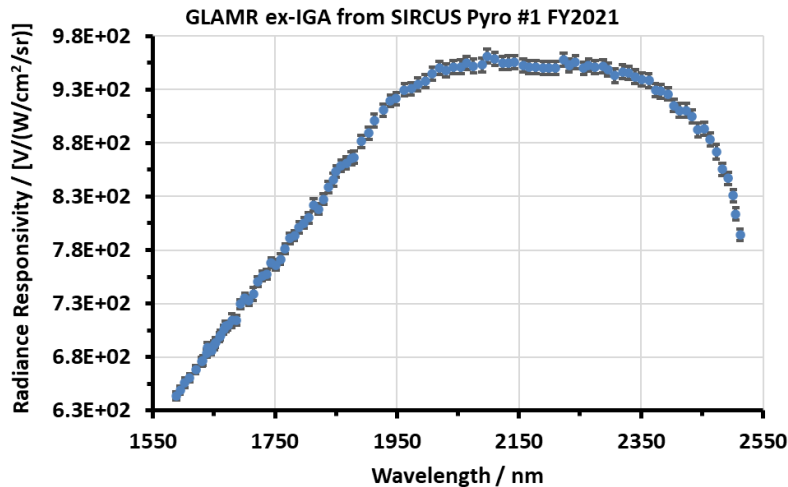

Figure 3.4 Absolute Spectral Radiance Responsivity of GLAMR exIGA from SIRCUS pyro #1 where the error bars represent the k=2 absolute uncertainty

Table 3.3: Tabulated absolute spectral radiance responsivity for GLAMR exIGA from SIRCUS pyro #1

Wavelength [nm]	Radiance Responsivity [V/(W/cm²/sr)]	Total k=1 Uncertainty (%)
1588.08	6.436E+02	0.30
1594.39	6.487E+02	0.30
1602.37	6.560E+02	0.34
1610.38	6.605E+02	0.30
1620.15	6.683E+02	0.30
1630.02	6.757E+02	0.31
1631.66	6.767E+02	0.32
1638.34	6.836E+02	0.31
1639.26	6.894E+02	0.31
1645.84	6.863E+02	0.31
1650.13	6.910E+02	0.31
1652.49	6.936E+02	0.31
1659.19	6.988E+02	0.31
1660.39	7.006E+02	0.32
1665.89	7.056E+02	0.32
1669.02	7.087E+02	0.34
1672.77	7.094E+02	0.31
1679.61	7.140E+02	0.44
1686.54	7.146E+02	0.31
1693.42	7.293E+02	0.30
1700.40	7.352E+02	0.31
1707.43	7.327E+02	0.31
1714.63	7.387E+02	0.43
1721.92	7.504E+02	0.30
1729.09	7.558E+02	0.31
1736.51	7.574E+02	0.30
1743.77	7.682E+02	0.31
1751.38	7.660E+02	0.32
1758.82	7.715E+02	0.32
1766.49	7.810E+02	0.30
1774.01	7.910E+02	0.31
1781.82	7.935E+02	0.31
1789.65	8.014E+02	0.33
1797.52	8.051E+02	0.32
1805.29	8.102E+02	0.31
1813.41	8.220E+02	0.35
1821.34	8.184E+02	0.31
1829.30	8.276E+02	0.31

1837.82	8.391E+02	0.32
1845.80	8.456E+02	0.35
1850.23	8.533E+02	0.33
1858.38	8.586E+02	0.32
1866.75	8.614E+02	0.34
1875.47	8.656E+02	0.35
1879.60	8.668E+02	0.32
1891.42	8.815E+02	0.33
1903.58	8.891E+02	0.31
1912.56	9.011E+02	0.33
1927.41	9.108E+02	0.32
1939.06	9.194E+02	0.31
1948.67	9.215E+02	0.32
1962.02	9.294E+02	0.31
1973.34	9.306E+02	0.31
1984.02	9.347E+02	0.32
1996.49	9.379E+02	0.32
2007.79	9.449E+02	0.32
2019.55	9.501E+02	0.33
2030.47	9.480E+02	0.32
2042.58	9.506E+02	0.32
2054.47	9.513E+02	0.33
2064.28	9.547E+02	0.33
2075.50	9.519E+02	0.33
2089.43	9.530E+02	0.34
2097.80	9.610E+02	0.34
2110.27	9.588E+02	0.33
2122.88	9.548E+02	0.33
2132.22	9.549E+02	0.34
2142.77	9.555E+02	0.34
2156.84	9.522E+02	0.33
2166.36	9.509E+02	0.32
2177.29	9.508E+02	0.33
2190.07	9.504E+02	0.32
2199.15	9.502E+02	0.32
2210.19	9.499E+02	0.32
2222.90	9.576E+02	0.31
2231.90	9.528E+02	0.32
2232.14	9.525E+02	0.32
2242.39	9.554E+02	0.32
2255.83	9.498E+02	0.30
2264.16	9.528E+02	0.32
2274.56	9.507E+02	0.32

2287.79	9.516E+02	0.33
2295.85	9.487E+02	0.32
2307.06	9.428E+02	0.33
2319.54	9.466E+02	0.35
2329.63	9.456E+02	0.33
2340.60	9.418E+02	0.34
2351.12	9.393E+02	0.33
2362.78	9.384E+02	0.34
2373.52	9.294E+02	0.32
2382.30	9.284E+02	0.35
2394.35	9.258E+02	0.32
2403.75	9.150E+02	0.33
2412.69	9.106E+02	0.35
2423.91	9.106E+02	0.34
2433.72	9.049E+02	0.33
2443.11	8.922E+02	0.35
2453.74	8.935E+02	0.34
2463.38	8.833E+02	0.34
2473.27	8.716E+02	0.39
2483.23	8.553E+02	0.35
2492.85	8.471E+02	0.34
2501.29	8.309E+02	0.34
2505.32	8.138E+02	0.37
2512.24	7.943E+02	0.35

Section 3.4 Uncertainty Analysis for the Radiance Responsivity of GLAMR exIGA

The uncertainty analysis for GLAMR exIGA is shown in Table 3.4 and includes the typical uncertainty components. Major contributors are the SIRCUS pyro #1 reference detector calibration and the distance uncertainty arising from the inverse square law measurements of the reference detector. In addition, the measurement standard deviation was significant at many individual points. Some individual points had high standard deviation around 0.2 % to 0.3 % but many points were less than 0.15 %.

It should also be noted that repeated measurements at select wavelengths resulted in higher standard deviations than is noted for the measurement standard deviation shown here. Individual measurements were comprised of 10-second waveforms, repeated 5 times for GLAMR exIGA and repeated 50 times to 100 times for SIRCUS pyro #1, depending on the signal level. Individual measurements generally resulted in standard deviation of 0.2 % to 0.3 % or less whereas repeat measurements generally had higher standard deviation ranging from 0.4 % to as high as 0.8 % at one wavelength. That repeating these individual measurements resulted in higher standard deviation could suggest some longer timescale drift compared to the individual measurement timescale. This is also indicated in the spectral data shown in Figure 3.4, where point-to-point

fluctuations are observed. Expansion of the uncertainty to the ~ 1 % level covers these fluctuations.

Table 3.4 Uncertainty Budget for Absolute Spectral Radiance Responsivity of GLAMR exIGA.

Uncertainty Component	Relative Standard Uncertainty [%]
	Radiance 1588 nm to 2512 nm
Combined Measurement Percent Standard Deviation[1]	0.13
Reference detector Irrad. Cal. (SIRCUS Pyro #1 from T-06 and Reflectance Dec 2020)[2]	0.28
Reference Detector Distance	0.09
Amplifier gain[3]	N.A.
Geometry Alignment	0.05
Aperture Areas[4]	0.03
Wavelength	0.02
Combined Standard Uncertainty (k=1)[5]	**0.33**

Note 1: This is the combined measurement percent standard deviation for the DUT, and reference detector averaged across the entire range. Values for individual wavelengths are provided in the calibration file. Some points had significantly high measurement percent standard deviation ~ 0.2 % to 0.3 % but most points were less than 0.15 % resulting in combined standard uncertainty of 0.3 – 0.4 depending on the measurement standard deviation at individual wavelengths.

Note 2: The pyro scale uncertainty varies with wavelength depending on the measurement uncertainty of the reflectance measurements. In general, the uncertainty of the reflectance was higher at shorter wavelengths towards 800 nm. Pyro scale uncertainty was 0.44 % from 900 nm to 940 nm, 0.37 % from 950 nm to 1000 nm, and 0.27 % above 1000 nm.

Note 3: There is no amplifier gain uncertainty. The reference pyro has an internal amplifier with a fixed gain that did not factor into the calculation. The DUT used the provided amplifier with the nominal gain setting 1×10^6 (1×10^5 with multiplier 10) which was not used in the analysis, so the uncertainty budget covers the total device (radiance meter and amplifier) with units of $[V/W/cm^2/sr]$.

Note 4: Combined uncertainty contributions for the reference detector and sphere apertures.

Note 5: This is not the full calibration uncertainty budget. The uncertainty budget, Table 3.4, does not include environmental effects on both the reference detector and the GLAMR radiometer. No evaluations of instrument performance characteristics such as temperature dependence, response linearity or temporal stability were performed. For customers who plan to interpolate the calibrated responsivity, estimates in the interpolated uncertainty can be determined according to reference 8.[8]

4. General Information

Information was recorded in the SIRCUS Vis #21 laboratory notebook, pp.59-67.

The calibration measurements, data analysis, and report writing were performed by Brian G. Alberding and John T. Woodward.

This calibration required 9 days of laboratory work (including setup, troubleshooting, and data collection) on SIRCUS and 7 days of data reduction, analysis, and reporting.

Significant experimental notes:

1. Previous calibrations of GLAMR exIGA utilized an extended IGA monitor detector placed on the optical table because no sphere mountable monitor detector was available for wavelengths greater than ~ 1700 nm. For this calibration, a MCT monitor detector mounted directly to the sphere was used to cover the entire wavelength range.

2. For the optical table holding the Argos (signal output) and IPG Cr^{2+}:ZnS/Se lasers a minor laser feedback issue was noticed. In normal operation, the wavelength measured by the wavemeter was observed to be unstable with fluctuations on the order of ~ 0.3 nm to 0.5 nm. If, however, the beam was blocked directly before the fiber input, the instability was removed with observed wavelength fluctuations less than 0.01 nm indicating possible laser feedback originating from the optical fiber back to the source laser. Slight misalignment of the fiber coupler angle did not appear to reduce the effect.

3. No Speckle control device was available to cover the wavelength range defined by the Argos (signal output) and IPG Cr^{2+}:ZnS/Se lasers. An attempt was made to utilize the ZrF_4 mode-mixer (GiGa) however, the device created enhanced laser feedback issues when activated (see point 2, above) with observed wavelength fluctuations of 1 nm to 2 nm or more.

4. Prior to the start of this calibration, there was a problem with the XY stage control. When the stage was moved too far towards the upper limit on the Y-axis, the stage would occasionally stall and/or lose track of home position and cause misalignment with the stage center positions. Details of the problem were evaluated on pg. 55 of the SIRCUS notebook. The detectors were set up to avoid moving the stage too far towards the limits on the y-axis. There was no obvious reason to suggest a similar problem occurred with the stage during this calibration.

5. The LabVIEW control program utilized for chopped data acquisition was updated from version 5 to version 6. This upgrade allowed for control of the DAQ voltage range for individual analog input channels (i.e. the optical voltage range could be set independently for each detector).

6. Background scattering measurements were taken (pg. 99) for SIRCUS pyro #1. In short, a one-inch diameter baffle was placed between the sphere and the source to block the radiation from the sphere as much as possible while still allowing the light to scatter within the box. The baffle was placed at various positions ranging from 13 cm to 18 cm away from the sphere source, with the sphere placed in the Z-position of the radiance responsivity measurements. A measurement of the SIRCUS Pyro #1 signal was measured with the baffle in place and again with the sphere source covered (to determine the floating background level of the pyroelectric detector). There was no significant contribution to the observed signal arising from scattering within the SIRCUS enclosure. The measurements with the baffle in place, after subtracting the contribution when the sphere was completely covered, represented less than 0.05 % of the signal.

Information about data files:

1. Full data files for the radiance responsivity of GLAMR exIGA are located on Elwood under:

   \\cfs2e.nist.gov\685\internal\G04\SIRCUS\SIRCUS\Calibrations\SIRCUS Calibrations\FY 2021 Calibrations\GLAMR\GLAMR exIGA

   Data file for the radiance responsivity of GLAMR IGA: "Radiance Responsivity GLAMR exIGA from SIRCUS pyro #1_FY2021.xlsx"

The files located in these directories are meant for internal NIST use only. Please do not distribute without authorization.

References

1. Brown, S. W., Eppeldauer, G. P. & Lykke, K. R. "Facility for spectral irradiance and radiance responsivity calibrations using uniform sources," *Appl. Opt.* **45**, 8218–8237 (2006).
2. Woodward, J. T. *et al.* "Invited Article: Advances in tunable laser-based radiometric calibration applications at the National Institute of Standards and Technology, USA," *Review of Scientific Instruments* **89**, 091301 (2018).
3. Houston, J. M. & Rice, J. P. "NIST reference cryogenic radiometer designed for versatile performance," *Metrologia* **43**, S31–S35 (2006).
4. Shaw, P.-S. "Report of Calibration for SIRCUS Si Trap Detectors T06 and T04 from 475 nm to 1000 nm," (2016).
5. Hanssen, L. M. "NIST Report of Calibration: 38075-S Special Tests Infrared Reflectance, Transmittance, and Emittance of Materials for Pyroelectric Detector Sample," Order Item No.: O-0000000712. (2020).
6. Cooksey, C. C. "NIST Report of Special Test (Revised): 38060S Spectral Diffuse Reflectance for Pyroelectric Detector Witness Sample," Order Item No.: O-0000000698-R. (2020).
7. Alberding, B. G. *et al.* "A pyroelectric detector-based method for low uncertainty irradiance and radiance calibrations in the short-wave infrared," *Applied Optics*, Accepted (2022). https://doi.org/10.1364/AO.455412.
8. Gardner, J. L. "Uncertainties in Interpolated Spectral Data," *J. Res. Natl. Inst. Stand. Technol.* **108**, 69–78 (2003).

Distribution Restrictions: None

This calibration report shall not be reproduced, except in full, without written approval by NIST.

Prepared by: Approved by:

_____   _____

Brian G. Alberding   Joseph P. Rice, Leader
Remote Sensing Group   Remote Sensing Group
Sensor Science Division   Sensor Science Division
Physical Measurement Laboratory   Physical Measurement Laboratory
(301) 975-4664   (301) 975-2133